Supporting information for: Wilson *et al.* 2022. The role of spatial structure on recovery of at-risk metapopulations. In: *Ecological Applications.*

Appendix S1: Overview of metapopulation model description & detailed results

Kyle L. Wilson[1,2]*, Alexandra C. Sawyer[1], Anna Potapova[1], Colin J. Bailey[1],Daniella LoScerbo[3,4], Elissa K. Sweeney-Bergen[1,5], Emma E. Hodgson[1,4], Kara J. Pitman[1], Karl M. Seitz[1], Lauren Law[1,6], Luke Warkentin[1,7], Samantha M. Wilson[1], William I. Atlas[1,8], Douglas C. Braun[3,5], Matthew R. Sloat[8], M. Tim Tinker[9], and Jonathan W. Moore[1,3]

[1]Earth to Ocean Research Group, Simon Fraser University
[2]Central Coast Indigenous Resource Alliance, Campbell River, BC
[3]Resource and Environmental Management, Simon Fraser University
[4]Fisheries & Oceans Canada, Cultus Lake Laboratory, Cultus Lake, BC
[5]Ministry of Forests, Lands, Natural Resource Operations, and Rural Development, Smithers, BC
[6]Fisheries & Oceans Canada, Salmonid Enhancement Program, Nanaimo, BC
[7]Fisheries & Oceans Canada, North Coast Stock Assessment, Smithers, BC
[8]Wild Salmon Center, Portland, OR
[9]Ecology and Evolutionary Biology, University of California Santa Cruz

21 November 2022

Contents

*Corresponding author - email: klwilson.ccira@gmail.com

1.1 Metapopulation model

1.1.1 Local & metapopulation dynamics

Our metapopulation was defined by a set of P local populations for a species with a one year generation time with time-dynamics that follows birth (i.e., recruitment R), immigration, death, and emigration processes typical to metapopulation theory and tested the role of multiple local and regional processes (Anderson et al. 2015; Fullerton et al. 2016; Zelnik et al. 2019; Bowlby & Gibson 2020; Okamoto et al. 2020):

$$N_{i,t} = (1 - d_{i,t})(R_{i,t} + \sum_{\substack{j=1 \\ j \neq i}}^{P} \omega p_{i,j} R_{j,t} - \omega R_{i,t}) \tag{S.1}$$

where $N_{i,t}$ was the number of adults in patch i at time t, $R_{i,t}$ was the number of recruits at time t, $\sum_{\substack{j=1 \\ j \neq i}}^{P} \omega p_{i,j} R_{j,t}$ was the number of recruits immigrating into patch i from any other patch, ω was the proportion of local recruits to disperse, $p_{i,j}$ was a distance-dependent dispersal function, and $d_{i,t}$ was the proportion of post-dispersal recruits lost from the disturbance regime.

Figure S1 shows how local patch recruitment at time t depended on adult densities at *t-1* and followed a reparameterized Beverton-Holt function based on compensation ratio (Box 3.1 in Walters & Martell 2004) and ignoring age-structure to model adult-to-adult dynamics, i.e., setting $\phi_{E_0} = 1$, $\phi_{B_0} = 1$ and $R_0 = N_0$ in Table 3 in Forrest et al. (2010):

$$R_{i,t} = \frac{\alpha_i N_{i,t-1}}{1 + \dfrac{\alpha_i - 1}{\beta_i} N_{i,t-1}} \epsilon_{i,t} \tag{S.2}$$

where α_i was the recruitment compensation ratio, β_i was local patch carrying capacity, and $\epsilon_{i,t}$ was lognormally distributed deviates to introduce stochastic recruitment dynamics.

Resource monitoring often occurs at the scale of the whole metapopulation by sampling aggregate abundances from multiple local populations to (Anderson et al. 2015; Moore et al. 2021), hence we define metapopulation adults as:

$$A_t = \sum_{i=1}^{P} N_{i,t} \tag{S.3}$$

with metapopulation recruits:

$$K_t = \sum_{i=1}^{P} R_{i,t} \tag{S.4}$$

Monitoring at the scale of the whole metapopulation can produce productivity relationships that aggregates the population dynamics and productivity among all local populations. For example, take a two patch metapopulation model (Figure S1) that each vary in demographic shape parameters $\alpha_1 = 2; \alpha_2 = 4$ and $\beta_1 = 100; \beta_2 = 200$. Here, recruitment compensation from local patches α_i gets averaged across the metapopulation leading to an average compensation ratio $\bar{\alpha}$ of 3. Likewise, the total carrying capacity of the metapopulation $\bar{\beta}$ becomes the summation of local patch carrying capacities $\sum \beta_i$, which was 300. This scale of monitoring generates the following local patch and metapopulation dynamics:
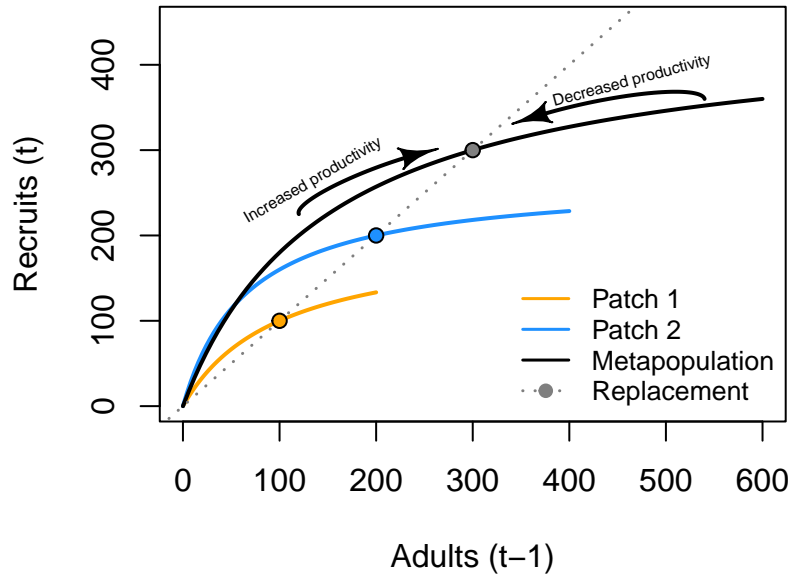
Figure S1: Density dependence in metapopulation and local patch recruitment dynamics. Dashed line indicates the line of replacement, with equilbrium indicated by points. When populations fall below equilibrium points, per-capita productivity improves driving populations back towards equilibrium. When populations exceed their capacity, per-capita productivity decreases driving populations back towards equilibrium. At each point of the x-axis, the distance between the solid and dashed lines indicates the amount of recruitment above replacement, i.e., the surplus recruitment produced via compensatory density dependence.

1.1.2 Creating the spatial networks

The next aspect to developing our metapopulation model was connecting the set of patches to one another (Yeakel et al. 2014). We needed to specify the number of patches, their arrangements (i.e., connections), and how far apart they are from one another. We followed some classic metapopulation and source-sink arrangements to create four networks that generalize across a few real-world topologies: a linear habitat network (e.g., coastline), a dendritic or branching network (e.g., coastal rivers), a star network (e.g., mountain & valley, or lake with inlet tributaries), and a grid network (e.g., grasslands).

To make networks comparable, each spatial network type needs the same leading parameters (e.g., number of patches P and mean distance between neighboring patches $\bar{d}$). In this case, we set P to `16` and $\bar{d}$ to `1` unit (distance units are arbitrary). We used the `igraph` package (Csardi & Nepusz 2006) to arrange our spatial networks as the following:
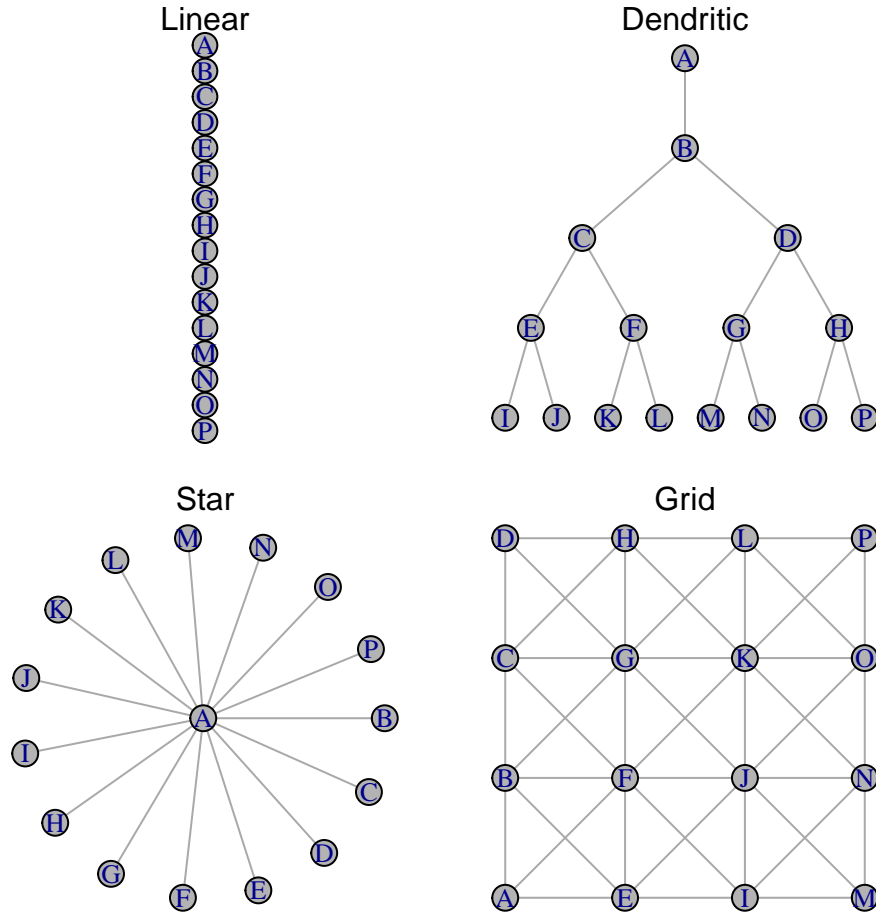
Figure S2: Four spatial network topologies.

Note that distances between neighbor patches in the above networks are equal. Table S1 shows an example dispersal matrix for a grid network.

1.1.3 Dispersal

Dispersal from patch i into patch j depends on constant dispersal rate ω (defined as the proportion of total local recruits that will disperse) and an exponential distance-decay function between i and j with distance cost to dispersal m (Anderson et al. 2015; Fullerton et al. 2016):

$$E_{i,j,t} = \omega R_{i,t} p_{i,j} \tag{S.5}$$

where $E_{i,j}$ was the total dispersing animals from patch i into patch j resulting from dispersal rate ω, total number of local recruits $R_{i,t}$, and probability of dispersal between patches $p_{i,j}$:

$$p_{i,j} = \frac{e^{-md_{i,j}}}{\displaystyle\sum_{\substack{j=1 \\ j\neq i}}^{P} e^{-md_{i,j}}} \tag{S.6}$$

where $d_{i,j}$ was the pairwise distance between patches, m was the distance cost to dispersal. The summation term in

Table S1: Example distance matrix between 16 patches within a grid network to affect distance-dependent dispersal rates.

	A	B	E	F	C	G	D	H	I	J	K	L	M	N	O	P
A	0	1	1	1	2	2	3	3	2	2	2	3	3	3	3	3
B	1	0	1	1	1	1	2	2	2	2	2	2	3	3	3	3
E	1	1	0	1	2	2	3	3	1	1	2	3	2	2	2	3
F	1	1	1	0	1	1	2	2	1	1	1	2	2	2	2	2
C	2	1	2	1	0	1	1	1	2	2	2	2	3	3	3	3
G	2	1	2	1	1	0	1	1	2	1	1	1	2	2	2	2
D	3	2	3	2	1	1	0	1	3	2	2	2	3	3	3	3
H	3	2	3	2	1	1	1	0	3	2	1	1	3	2	2	2
I	2	2	1	1	2	2	3	3	0	1	2	3	1	1	2	3
J	2	2	1	1	2	1	2	2	1	0	1	2	1	1	1	2
K	2	2	2	1	2	1	2	1	2	1	0	1	2	1	1	1
L	3	2	3	2	2	1	2	1	3	2	1	0	3	2	1	1
M	3	3	2	2	3	2	3	3	1	1	2	3	0	1	2	3
N	3	3	2	2	3	2	3	2	1	1	1	2	1	0	1	2
O	3	3	2	2	3	2	3	2	2	1	1	1	2	1	0	1
P	3	3	3	2	3	2	3	2	3	2	1	1	3	2	1	0

the denominator normalizes the probability of moving to any patch to between 0 and 1 with the constraint that dispersers cannot move back into their home patch (i.e., $j \neq i$. With $\bar{d} = 1$, $m = 0.5$, $\omega = 0.1$, $R_{i,t} = 100$ in a linear network):
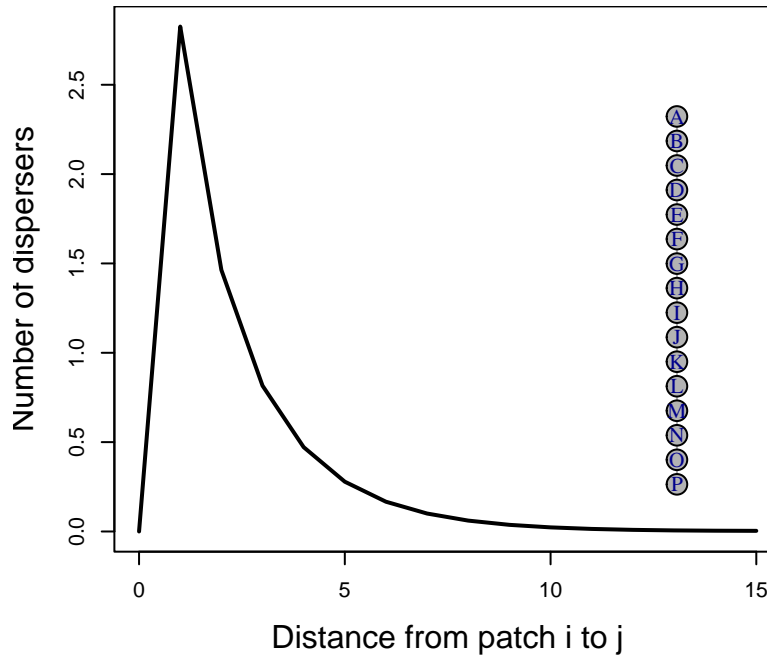

Figure S3: Example dispersal patterns across linear network.

1.1.4 Disturbance regimes

In all scenarios, disturbance was applied after 50 years of equilibrating the metapopulation at pristine conditions. We then applied a pulsed disturbance regime at year 50 (the regime varied from *uniform, localized, even,* and

78 *localized, uneven* - see *Scenarios* below). Disturbance immediately removed a fixed proportion of the
79 metapopulation adults at that time (i.e., `0.9` of $A_{t=50}$). Once applied, the metapopulation was no longer disturbed
80 and spatio-temporal recovery dynamics emerged from these conditions given the ecological scenarios of network
81 complexity, dispersal rate, spatio-temporal correlations, local patch demographics, and magnitude of stochastic
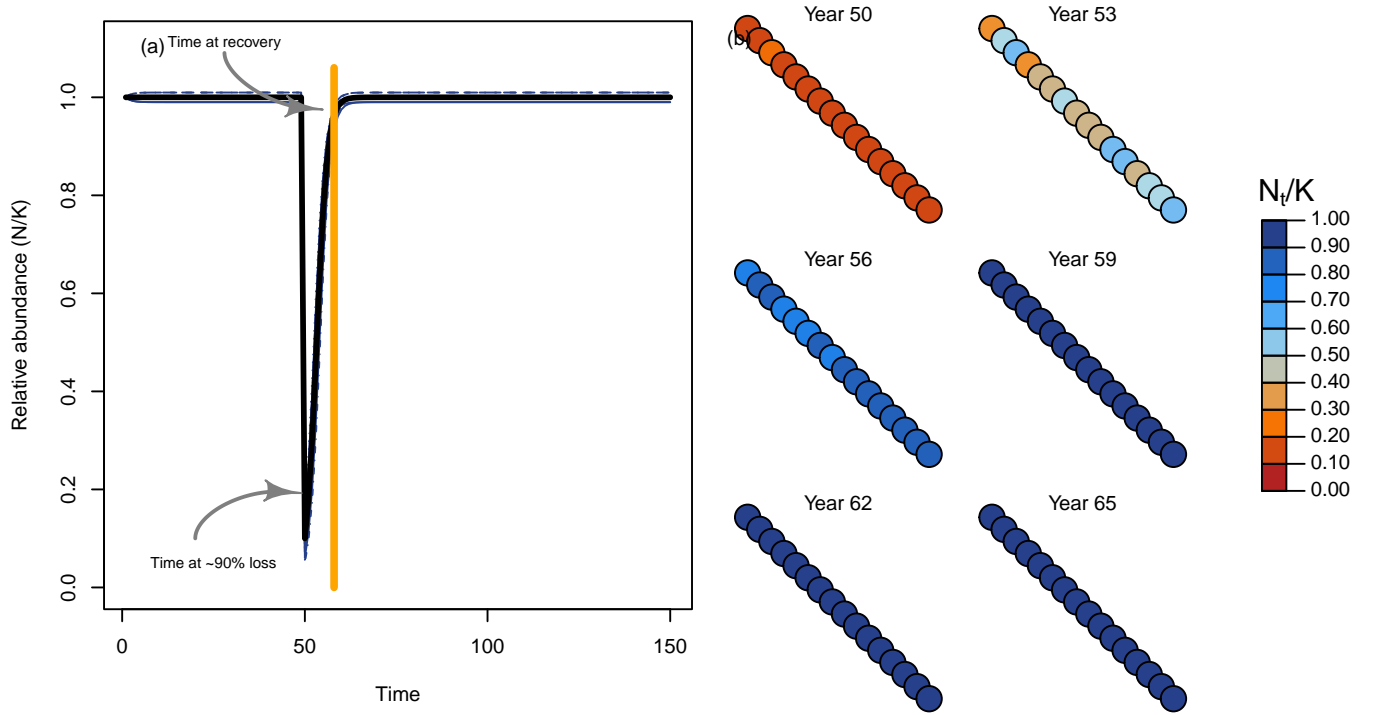82 variance.

Figure S4: Recovery regime of metapopulation with linear topology through time (a) and space (b).

83 **1.1.5 Recruitment stochasticity**

84 Our model allowed for stochastic recruitment that followed a lognormal distribution with average variation in
85 recruitment of σ_R. In cases with stochastic recruitment, the deterministic recruitment in eq. S.4 becomes:

$$R_{i,t} = \frac{\alpha_i N_{i,t-1}}{1 + \dfrac{\alpha_i - 1}{\beta_i} N_{i,t-1}} e^{(\epsilon_{i,t} - \frac{\sigma_R^2}{2})} \tag{S.7}$$

86 where lognormal deviates for each patch i at time t were drawn from a multivariate normal distribution (MVN)
87 with bias correction $\dfrac{\sigma_R^2}{2}$. If σ_R was low, then metapopulation dynamics approach the deterministic case. In some
88 scenarios, we evaluated the role of spatially and/or temporally correlated deviates among local patches to model
89 potential common drivers affecting metapopulation dynamics (e.g., Moran effects). Expected recruitment deviates
90 followed a first-order autoregression model such that:

$$\epsilon_{i,t} = \rho_T \epsilon_{t-1} + MVN(\mu = 0, \Sigma = \sigma_R^2(1 - \rho_T^2)e^{(-\rho_S D_{i,j})}) \tag{S.8}$$

where ρ_T was temporal correlation (bounded $0-1$) and ρ_S was rate of distance-decay in spatial correlation
(bounded $0-\infty$ with higher values leading to independent patches). If ρ_T was 0 and ρ_S was high, then annual
recruitment deviates were independent. We modelled the initial conditions for autoregressive recruitment deviates

$\epsilon_{i,1}$ by drawing from a stationary normal distribution with mean $\mu = 0$ and variance σ_R^2 such that:

$$\epsilon_{i,1} \sim N(\mu = 0, \sigma = \sigma_R) \tag{S.9}$$

We illustrate the effects of four kinds of recruitment deviates below using the same random number generator seed:
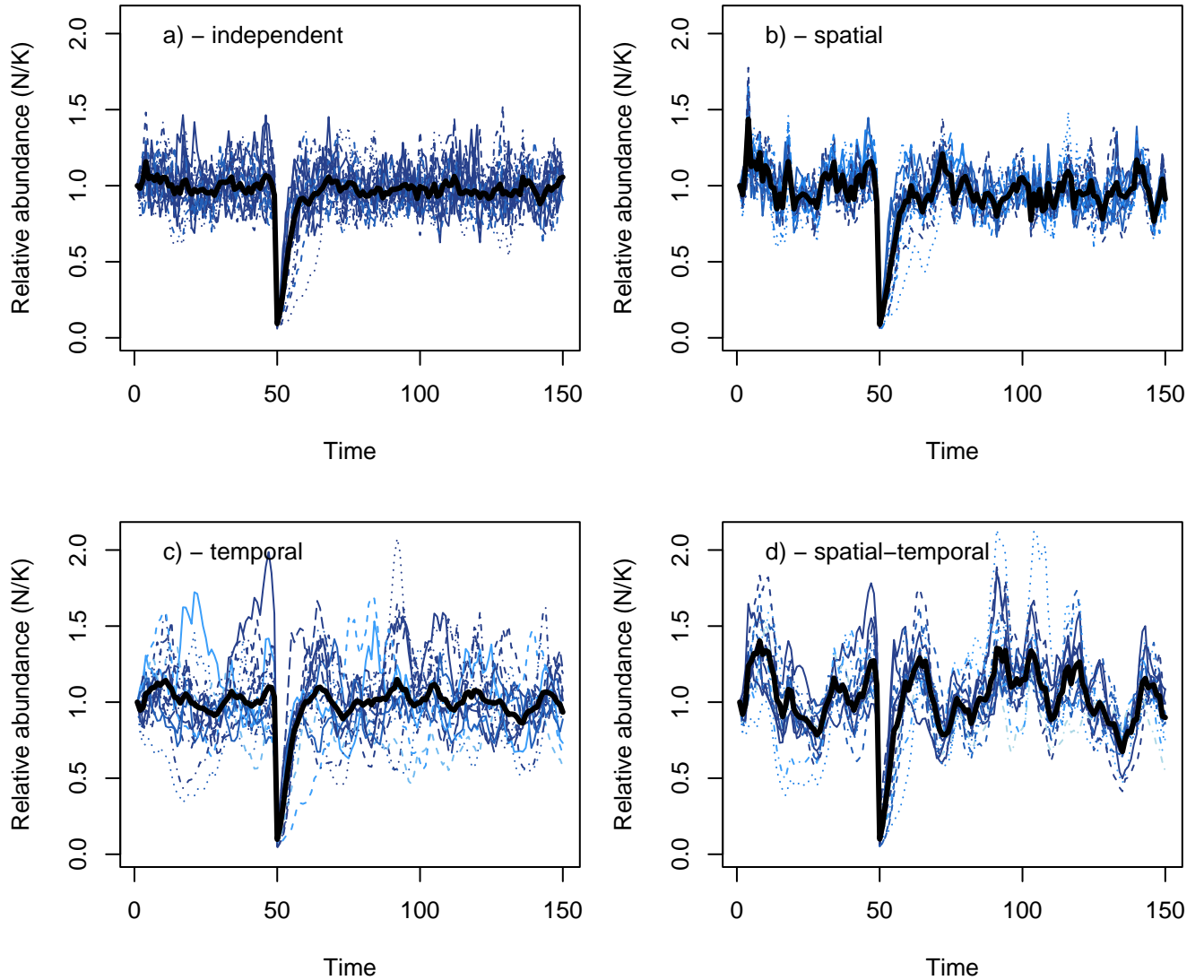

Figure S5: Metapopulation dynamics with independent (a), spatially correlated (b), temporally correlated (c), and spatio-temporally correlated (d) recruitment deviates. Black line indicates metapopulation, and dashed lines indicate local patches with red and blue relating to abundances after 100 years post-disturbance were less than or greater than 1.0 pre-disturbance, respectively.

1.2   Post-disturbance outcomes

1.2.1   Monitoring & management at aggregate-scale

While true metapopulation dynamics emerge from local patch dynamics and dispersal in eq. S.1, natural resource managers often monitor and manage at the scale of the metapopulation. Hence, management at this scale inherently defines the stock-recruitment dynamics of the aggregate complex of patches (i.e., metapopulation) as:

$$\mathbb{E}(N_t) = \frac{\bar{\alpha}A_{t-1}}{1 + \dfrac{\bar{\alpha}-1}{\bar{\beta}}A_{t-1}} \tag{S.10}$$

where $\bar{\alpha}$ was the compensation ratio averaged across the metapopulation and $\bar{\beta}$ was the carrying capacity summed across the entire metapopulation.

1.2.2 Recovery metrics

We measured the following post-disturbance outcomes to track the temporal and spatial recovery regime of the metapopulation.

1. Recovery rate after disturbance: Recovery rate represents the proportional post-disturbance recovery towards metapopulation carrying capacity gained per year (1 year = 1 generation in our models). Recovery rate was calculated as $1 - T_{recovery}/T_{sim}$ where the recovery time, $T_{recovery}$, was the number of years/generations it took for the metapopulation to reach five consecutive years   pre-disturbance abundance. Recovery rate captures how quickly the aggregate metapopulation recovers from disturbance but doesn't take into account whether any given local patches recover to their pre-disturbance capacity nor did it allow for any uncertainty around recovery criteria.

2. Patch occupancy: The mean number of patches with `>0.1` local carrying capacity after disturbance in the short-term (5 years), medium-term (10 years), and long-term (25 years). This value characterizes the expected risk of spatial contractions or local patch collapses, and reflects how interactions between spatial structure, disturbance, and dispersal shape source-sink dynamics and the ability to provide (or not) rescue effects and recover local patches.

3. Relative production: The ratio between the empirical metapopulation adult abundances to the expected adult recruitment if the metapopulation were a single, contiguous population of equivalent size and productivity (i.e., carrying capacities and productivity were equal to the sum β and mean α among patches, respectively). We term Δ_N by calculating the stock-recruitment model to aggregate metapopulation adults (eq. S.10) such that:

$$\Delta_{N_t} = \frac{A_t}{\mathbb{E}(N_t)} \tag{S.11}$$

   A value of 1.0 would indicate that the disturbed metapopulation production was equal to a single, contiguous population such that source-sink dynamics were not consuming surplus recruits. In other words, this metric can describe whether the metapopulation acts more than ($\Delta_{N_t}>1.0$), less than ($\Delta_{N_t}<1.0$), or equal to the sum of its parts ($\Delta_{N_t}=1.0$).

4. Risk of non-recovery after disturbance: Non-recovery rate was defined as the % of simulations where metapopulation abundance failed to recover to `1.0` of the average pre-disturbance abundance for `5` consecutive years post-disturbance. This "non-recovery rate" reflects the risk of a long-term state shift in metapopulation dynamics after disturbance in the face of stochasticity.

1.3 Scenarios

We tested all combinations of the following eight processes (below) and ran `100` stochastic iterations per scenario (see section on *Sensitivity test of mean recovery metrics* below) to estimate the mean outcome for each of the above recovery metrics:

1. Homogenous and spatially variable recruitment compensation ratio across patches, i.e. intrinsic rate of population growth (α_i).

   a. when *variable*, $\alpha_i \sim TN(\mu = \bar{\alpha}, \sigma_\alpha = 0.3\bar{\alpha})$ with a truncation applied such that $5 \leq \alpha_i \geq 1$ to ensure that patches could, at minimum, could replace themselves but with an upper limit of a 5-fold improvement to per-capita productivity. By comparison, Myers et al. (1999) found that compensation

136   ratio (their $\hat{\alpha}$) ranged 1-7 for most fish species. Since our focus was on at-risk species, we opted to
137   truncate this range towards the lower limit, with a mean of `2.0`.

2. Homogenous and spatially variable local carrying capacity across patches, i.e. asymptote of expected recruits
   at high adult densities (β_i)

   a. when *variable*, $\beta_i \sim multinomial(p_i, N)$ where $p_i = \dfrac{e^{\theta_i}}{\sum e^{\theta_i}}$, $\theta_i \sim uniform(0, 1)$, and $N = \bar{\beta}$ - with the
      added constraint that $\beta_i < 0.1\bar{\beta}$ to ensure that no one patch exceed 10% of total metapopulation
      abundance (a necessary constraint when modelling *local, even* and *local, uneven* disturbances below).
      Note that, when local variation in demography rates occurred, the truncated normal in *Appendix S1:*
      Section 1.3.1.a and truncated multinomial in *Appendix S1: Section 1.3.2.a* above led compensation ratio
      and carrying capacity, respectively, to vary by the same magnitude ~28% coefficient of variation
      (Appendix S1: Figure S6).

3. Disturbances where a proportion of individuals removed from metapopulation (e.g., `0.90`) occurs.

   a. *uniform* - random individuals removed at equal vulnerability across all patches.
   b. *local, even* - random individuals removed from randomly selected subset of patches (as long as the target
      individuals lost in the metapopulation can be achieved in that subset of patches)
      i. Specifically, a numerical algorithm was used to search and find a set of disturbance conditions
         whereby removing a random proportion of individuals from a random subset of local patches
         achieved both:
         - total loss summed to a ~90% loss in abundance to the whole metapopulation, and
         - left at least one local patch *undisturbed* to start metapopulation recoveries.
   c. *local, uneven* - total extirpation of randomly selected subset of patches (as long as the target individuals
      lost in the metapopulation can be achieved in that subset of patches).
      i. Specifically, a numerical algorithm was used to search and find a set of local demographic conditions
         whereby extirpations to a random subset of local patches that achieved both:
         - total loss summed to a ~90% loss in abundance to the whole metapopulation, and
         - left at least one local patch *undisturbed* to start metapopulation recoveries.

4. Density-independent dispersal rates ω from 0 to 5% of individuals within a patch will disperse.

5. Topology of the spatial networks with linear, dendritic, star, and grid networks. Each network with $P = 16$
   and distance between patches $\bar{d} = 1$.

6. Stochastic recruitment deviates with low, medium, and high standard deviation in lognormal error. Used to
   generate stochastic population dynamics via random deviates from the expected recruitment relationship in
   eq. S.2.

7. Temporal correlation in recruitment deviates from low, medium, and high correlation (i.e., good year at time
   t begets good year at time *t+1*).

8. Spatial correlation in recruitment deviates among patches from low, medium, to high correlation (i.e.,
   neighboring patches go up or down together).

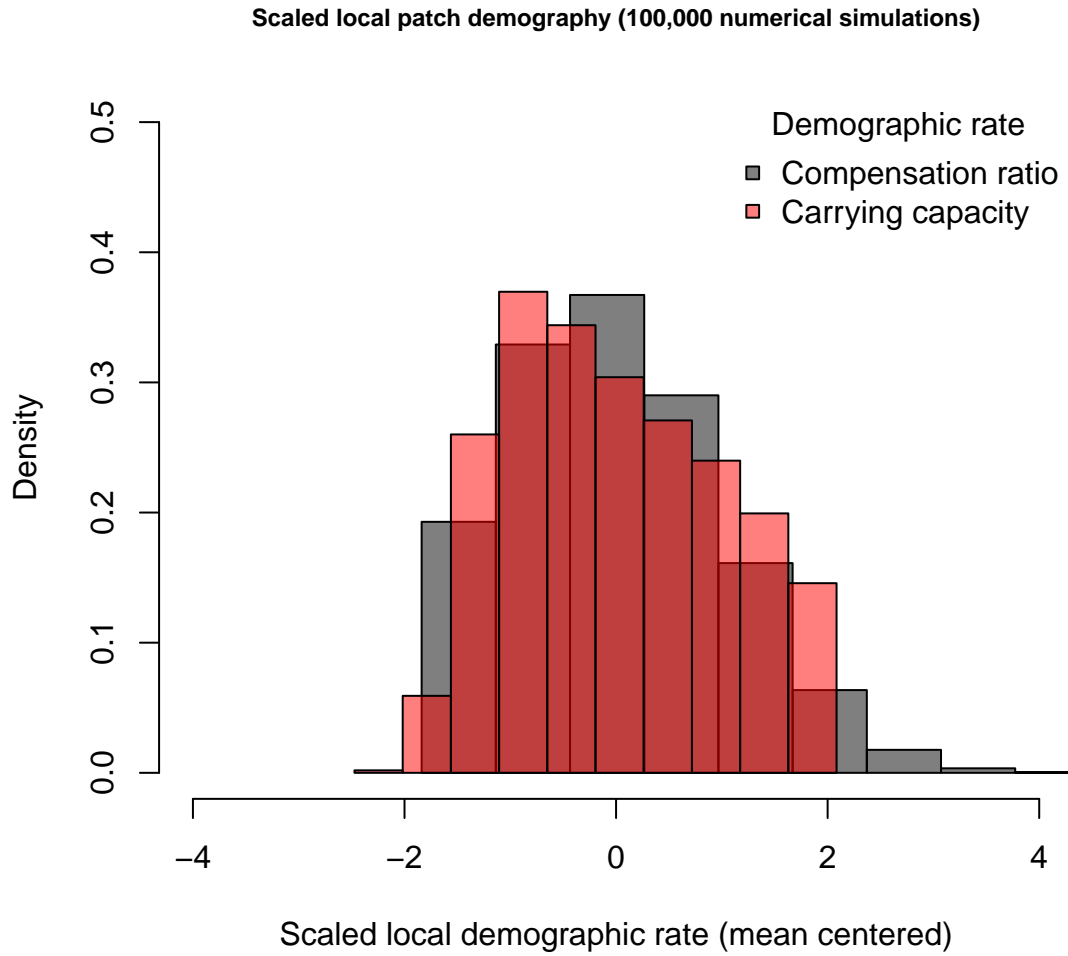**Scaled local patch demography (100,000 numerical simulations)**

Figure S6: Histogram showing variation among demographic rates after simulatng 100,000 local patches when using the truncated normal in Appendix S1: Section 1.3.1.a and truncated multinomial in Appendix S1: Section 1.3.2.a when modelling variation in local compensation ratio (grey) and carrying capacity (red).

1.3.1 Example results

We demonstrate our metapopulation model with an example outcome for a linear network composed of `16` patches, a dispersal rate of `0.01` and a high enough dispersal cost such that individuals are only willing to move to their closest neighboring patches. This limits the strength of potential rescue effects. For this example, patches varied in their productivity and carrying capacity but will have deterministic population dynamics.
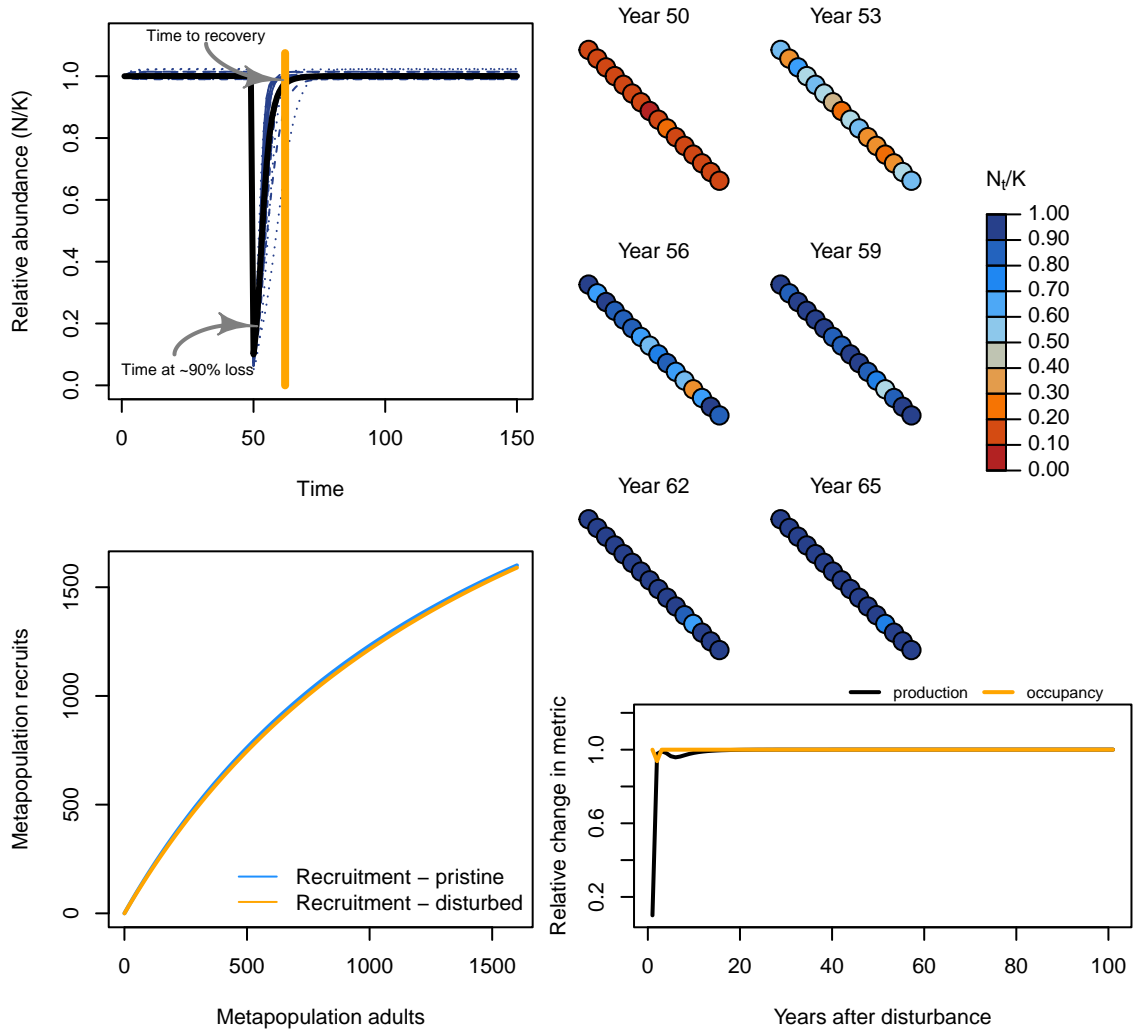
Figure S7: Example iteration of spatial recovery regime of metapopulation with linear topology through time (top left) and space (top right). Recruitment dynamics before and 10 years after disturbance (bottom left). Relative bias in aggregate-scale estimates of carrying capacity, compensation ratio, and recruitment production in recovery phase (bottom right).

177   We can then contrast this with a different network shape, like a dendritic network.
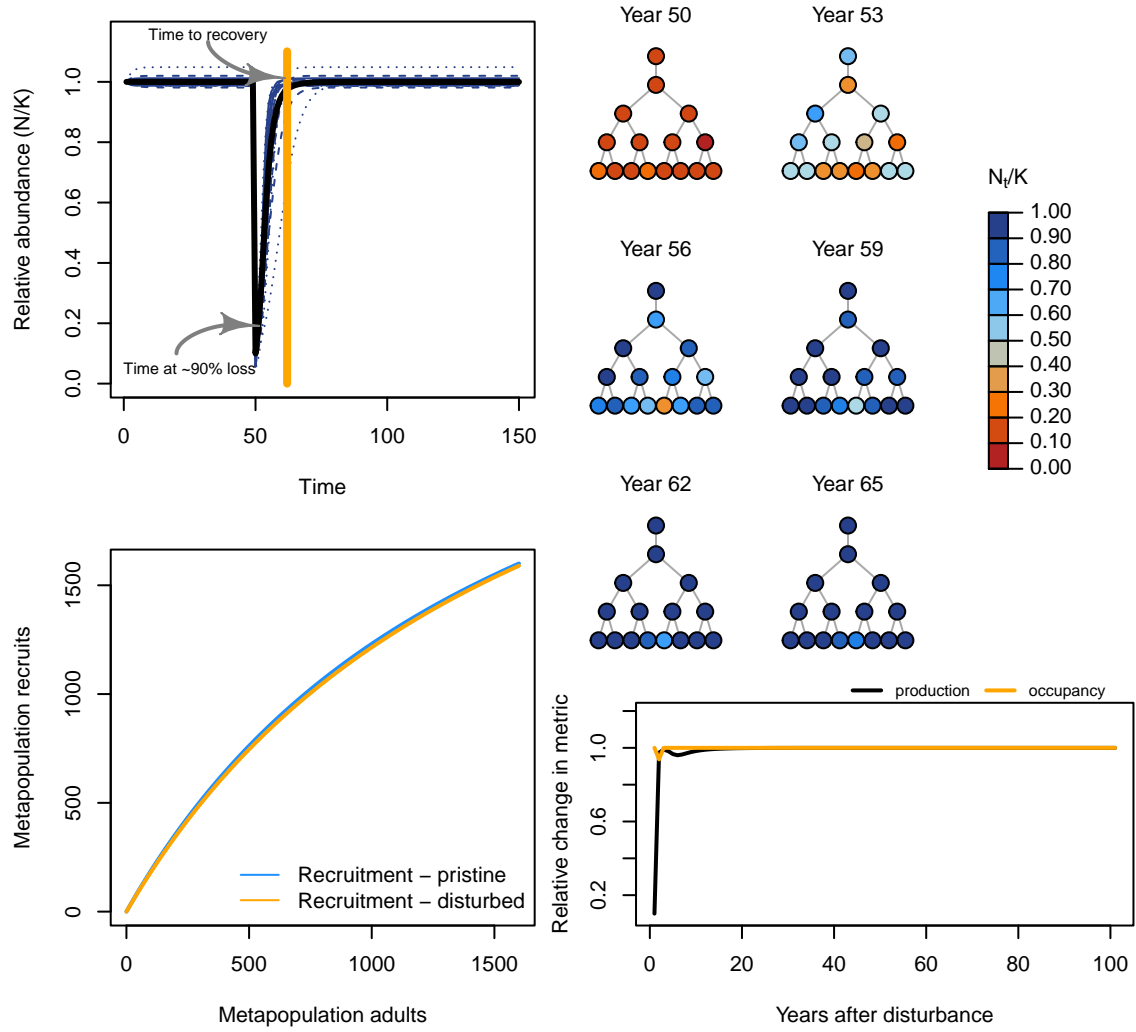

Figure S8: Example iteration of spatial recovery regime of metapopulation with dendritic topology.

178 Now, let's add some stochasticity to recruitment and see how this affects the recovery regime.
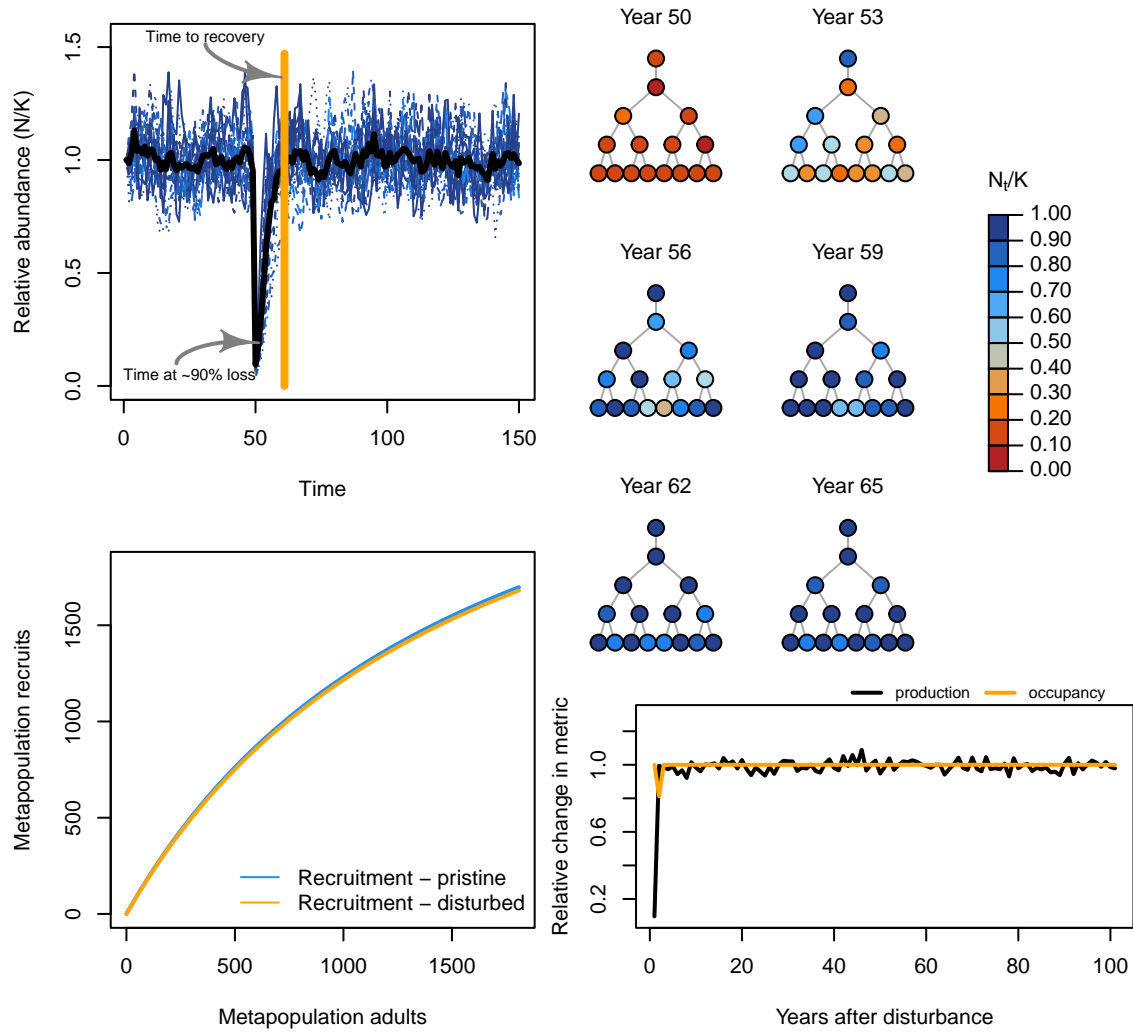

Figure S9: Example iteration of spatial recovery regime of stochastic metapopulation.

179 Next, we can contrast with a disturbance regime where the disturbance is concentrated on local patches that can
180 be completely extirpated (rather than the disturbance being applied proportionally across all patches e.g., a
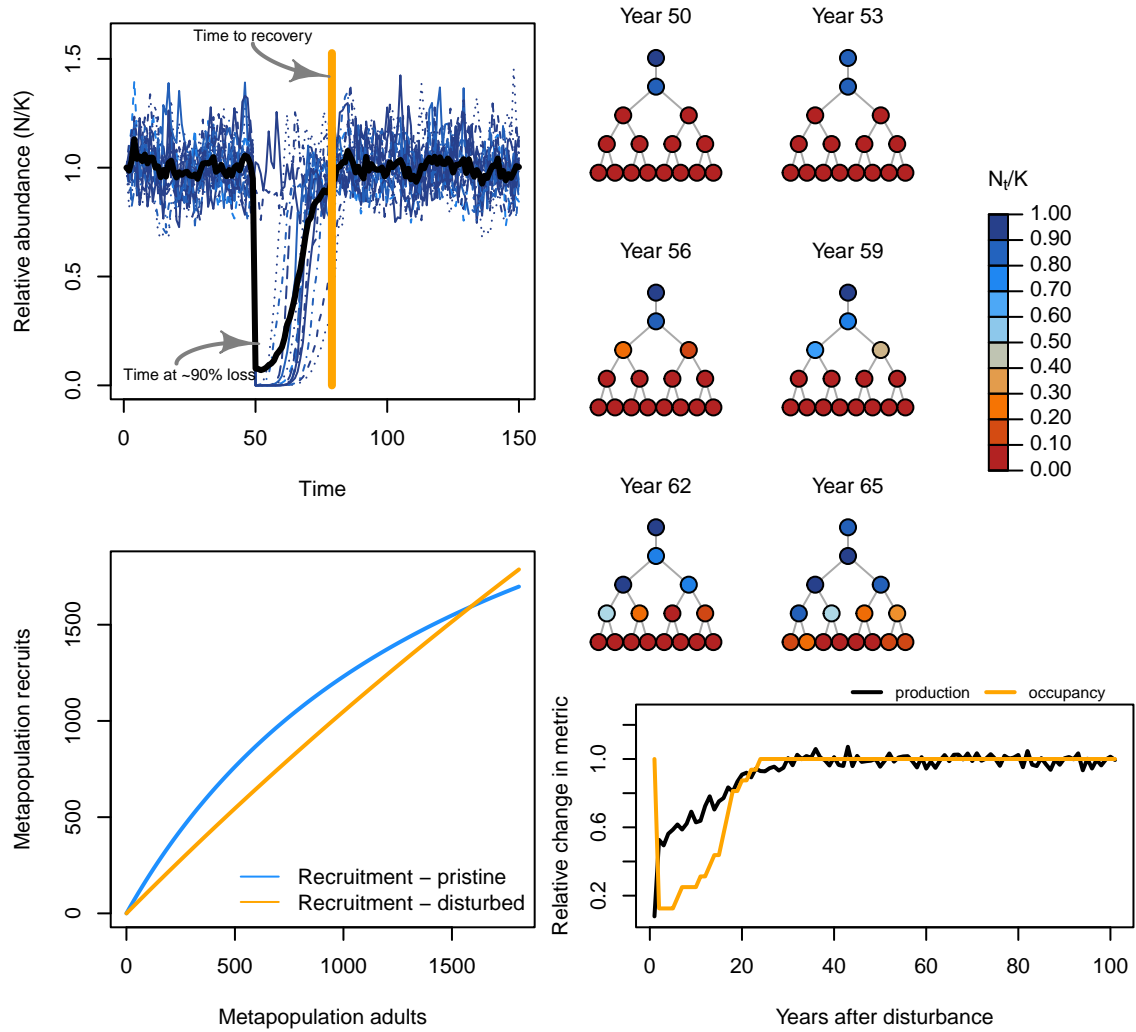181 mixed-stock fishery).

Figure S10: Example iteration of spatial recovery regime of stochastic metapopulation.

1.4   Sensitivity test of mean recovery metrics

The total number of scenarios resulted in a long computation time to run all simulations a large number of times
necessary to evaluate how metapopulation responded, on average, to our ecological and disturbance scenarios. To
determine a sufficient number of bootstrap iterations to run, we ran a sensitivity test to explore the relative
sensitivity of the mean for a few recovery metrics of interest (recovery rate) to the number of stochastic simulations
ran per scenario. Below, we repeated the scenario for a metapopulation with a dendritic network, with high
stochasticity, locally uneven disturbances, large spatial-temporal correlations, variable patch productivities, and
variable patch capacities along gradients of 10, 100, 500, and 1,000 stochastic simulations. Based on these
preliminary results, we see that the mean for most metrics was relatively insensitive with at least 100 simulations.
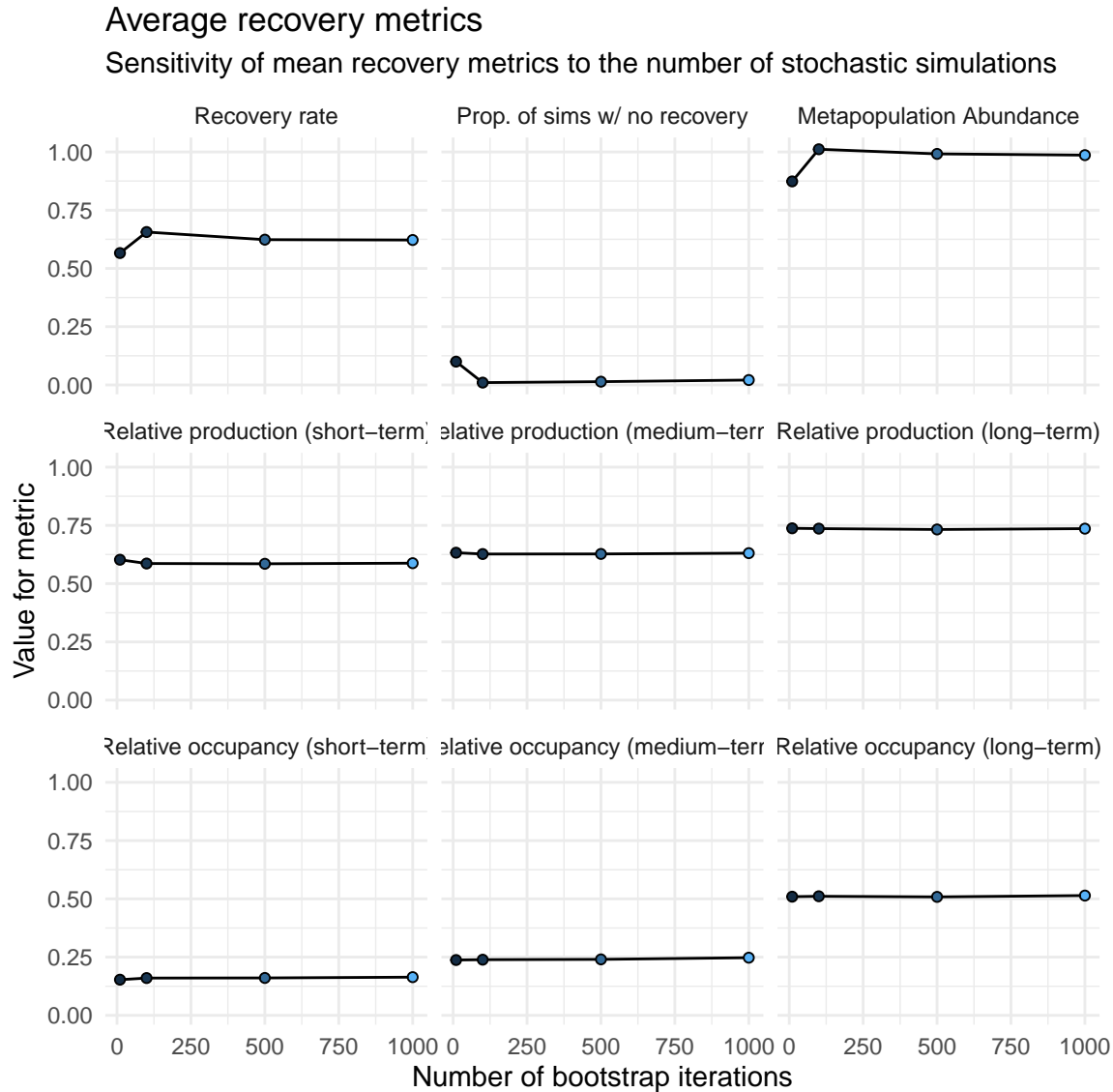

Figure S11: Sensitivity test of mean recovery metrics to number of iterations to bootstrap the stochastic simulations.
Example metapopulation consisted of a dendritic network, high recruitment stochasticity, locally uneven disturbance
regime, large spatial-temporal correlations, variable patch productivities, and variable patch capacities tested along
gradients of 10, 100, 500, and 1,000 bootstrapped iterations.

1.5 General patterns

1.5.1 Effects of disturbance regime

The strongest lever influencing recovery in our simulated metapopulations was, by far, the characteristics of the disturbance regime. Specifically, the degree to how locally concentrated the disturbance was on the set of patches was more influential than variable density dependence, dispersal rates, or network topology. Localized disturbances increased the risk of spatial contraction, reduced recovery rates and aggregate compensation, and increased the risk of non-recoveries. By altering aggregate compensation, localized disturbance reduced the relative production of the metapopulation. In other words, through changes in source-sink dynamics, metapopulations under localized disturbance acted less than the sum of their parts – the more localized the impacts, the worse these effects. Uniform disturbances generally left the metapopulation dynamics unaffected with few changes to recovery metrics outside of occasionally slower recoveries. These above spatial and temporal recovery processes also appeared tied to one another such that changes to any of them had feedbacks with other recovery metrics. Perhaps intuitively, for example, patch occupancy was highly correlated to the relative production of the metapopulation, such that the more patches occupied, the more that metapopulation dynamics resembled a contiguous population.
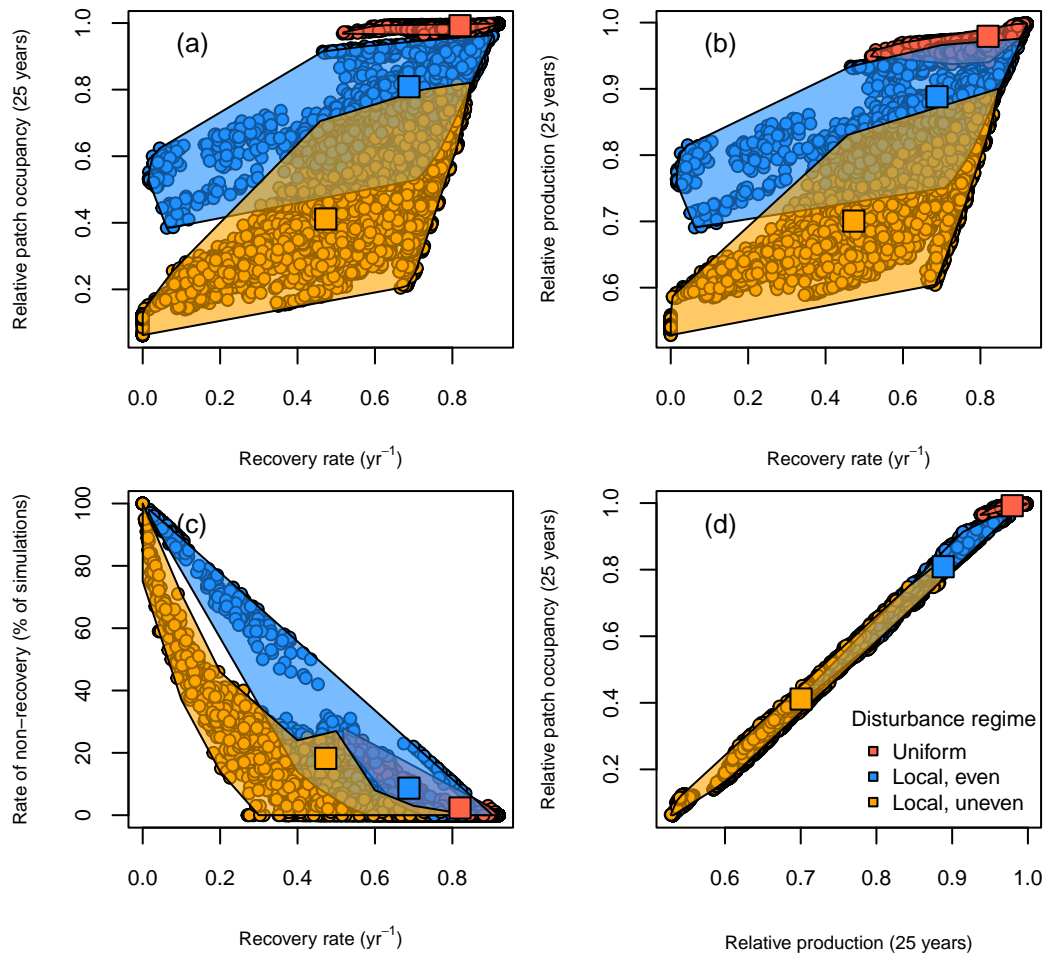

Figure S12: The role of spatial disturbance regimes on metapopulation recoveries and covariation among four recovery metrics: (a,b,c) recovery rate – the annual rate of metapopulation recovery; (a,d) relative patch occupancy – the mean proportion of patches occupied 25 years after disturbance; (b,d), relative production – the ratio between the summed abundances across all patches to the expected production of an equivalent single population 25 years after disturbance; and (c) rate of non-recovery – the percent of 100 stochastic simulations where the metapopulation failed to recover. Each point represents a single simulation for a metapopulation under a unique combination of local productivity, dispersal, spatial network, stochasticity, and disturbance (9,504 total simulations). Shaded regions describe the range in recovery metrics for all simulated metapopulations and are colored by disturbance regime. Square points represent the mean recovery metrics from all simulations within each disturbance regime.

₂₀₅ **1.5.2 Role of network structure & dispersal**

₂₀₆ We now show some general patterns in how variable patch demographic rates, network structure, dispersal,
₂₀₇ disturbance, recruitment stochasticity, and spatio-temporal correlations variation affects metapopulation *recovery*
₂₀₈ *rates* (shown in Figures 4 and 5 of the main text), *non-recovery rate* (i.e, the number of simulations where the
₂₀₉ metapopulation fails to recover), *patch occupancy* (i.e., number of patches with local abundance <10% of
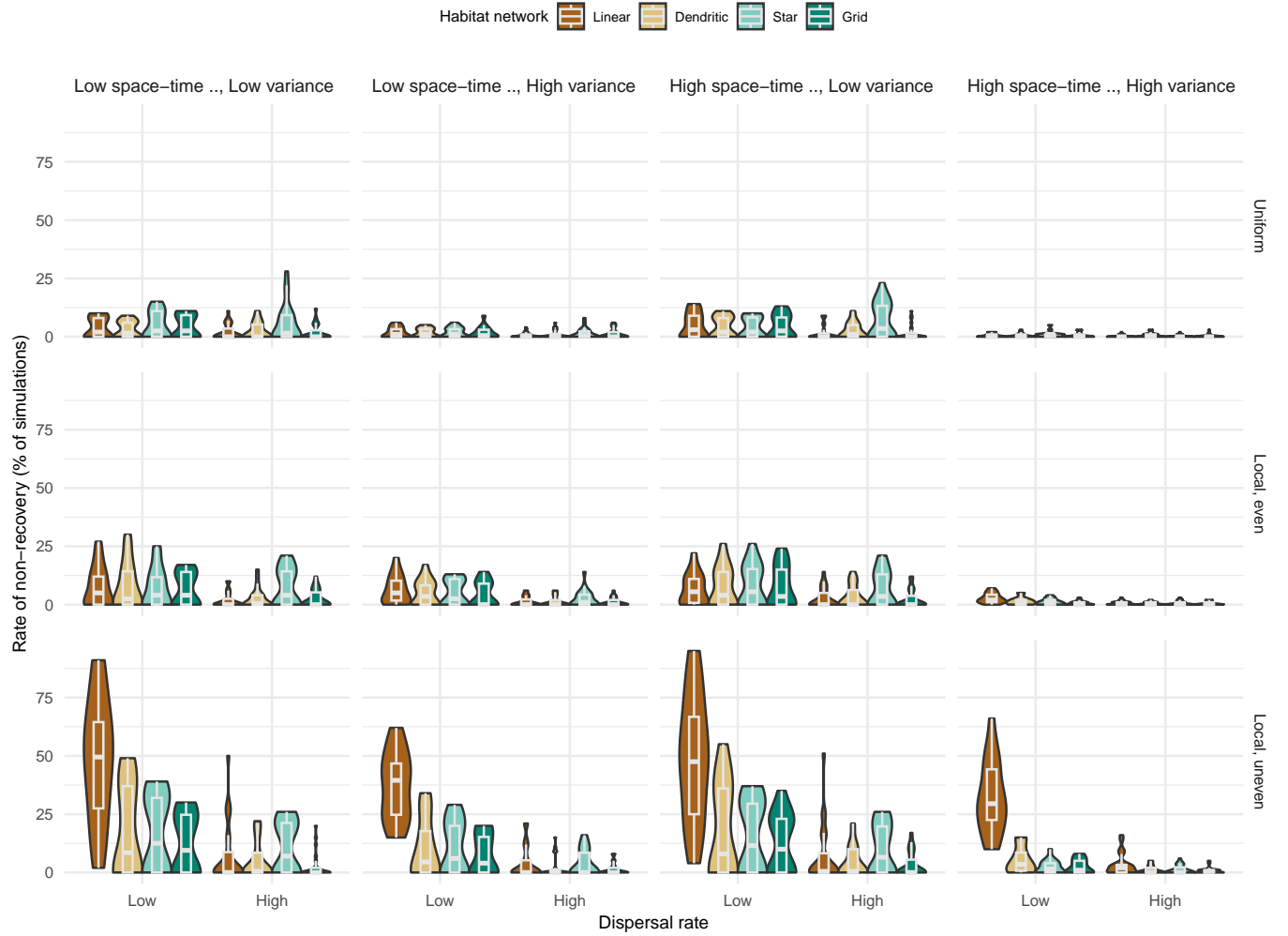₂₁₀ pre-disturbance), and *relative production*.

Figure S13: Violin plots showing distribution of the risk of non-recovery for metapopulations along gradients of
network configuration, dispersal categories (low 0.001; high>0.001), stochasticity (low=0.001; high=0.1, spatial-
temporal correlations (low 0; high=0.6), and spatial distribution of disturbance.

₂₁₁ Next, we show violin plots demonstrating the long-term impacts to patch occupancy.
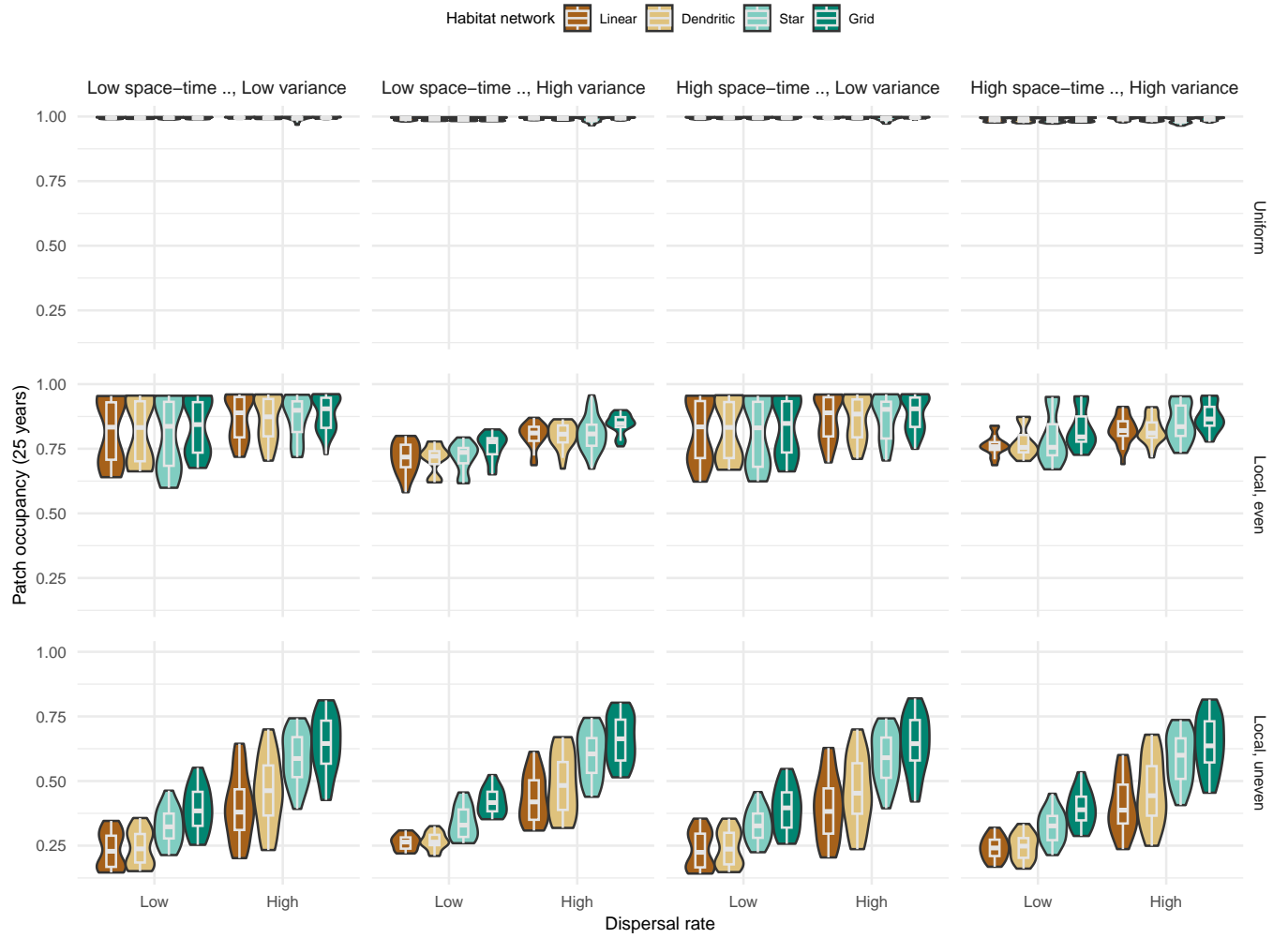
Figure S14: Violin plots showing distribution of patch occupancies for metapopulations along gradients of network configuration, dispersal categories (low 0.001; high>0.001), stochasticity (low=0.001; high=0.1, spatial-temporal correlations (low 0; high=0.6), and spatial distribution of disturbance.

Next, we show variation in relative production metrics. Figure S10 shows the tight correlation between patch occupancy and relative production. Hence, Figure S12 and S13 look quite similar.
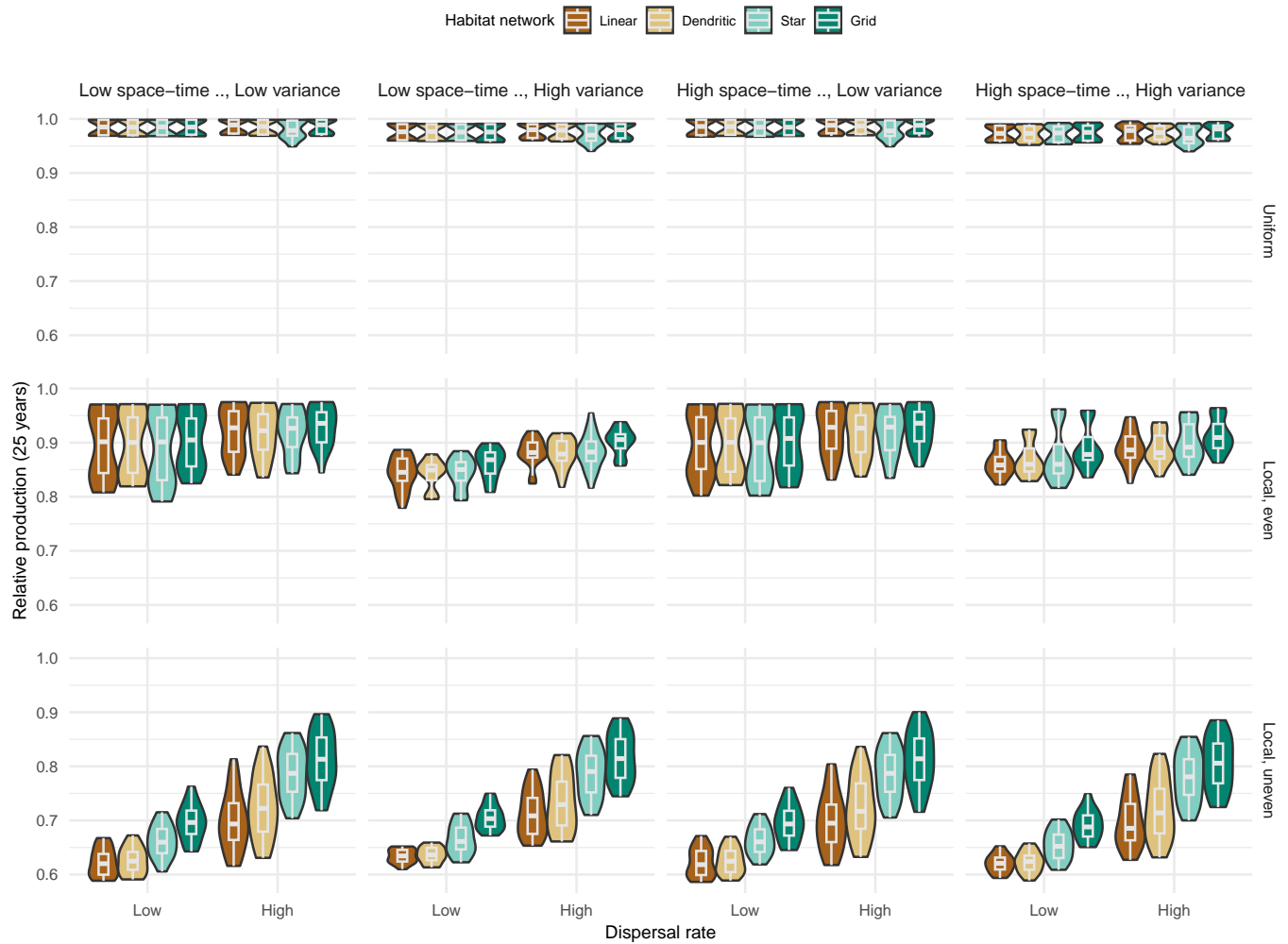
Figure S15: Violin plots showing distribution of relative production for metapopulations along gradients of network configuration, dispersal categories (low 0.001; high>0.001), stochasticity (low=0.001; high=0.1, spatial-temporal correlations (low 0; high=0.6), and spatial distribution of disturbance.

Dispersal, landscape structure, and local density-dependence also affected metapopulation recovery patterns in three key ways, though to a lesser extent. First, recovery rates increased with increased dispersal. However, this effect was nonlinear with diminishing benefits of dispersal occurring at ~1-3%, depending on spatial structure and disturbance. Second, more linearized networks had slower recovery times than more connected networks suggesting that rescue effects take some time to cascade through the entire network of patches; but this interacted with the disturbance regime as only local, extirpation exhibited this change in any substantial manner. Last, diversity in local patch compensation and carrying capacities tended to slow metapopulation recoveries - this effect interacted with other factors like stochasticity.
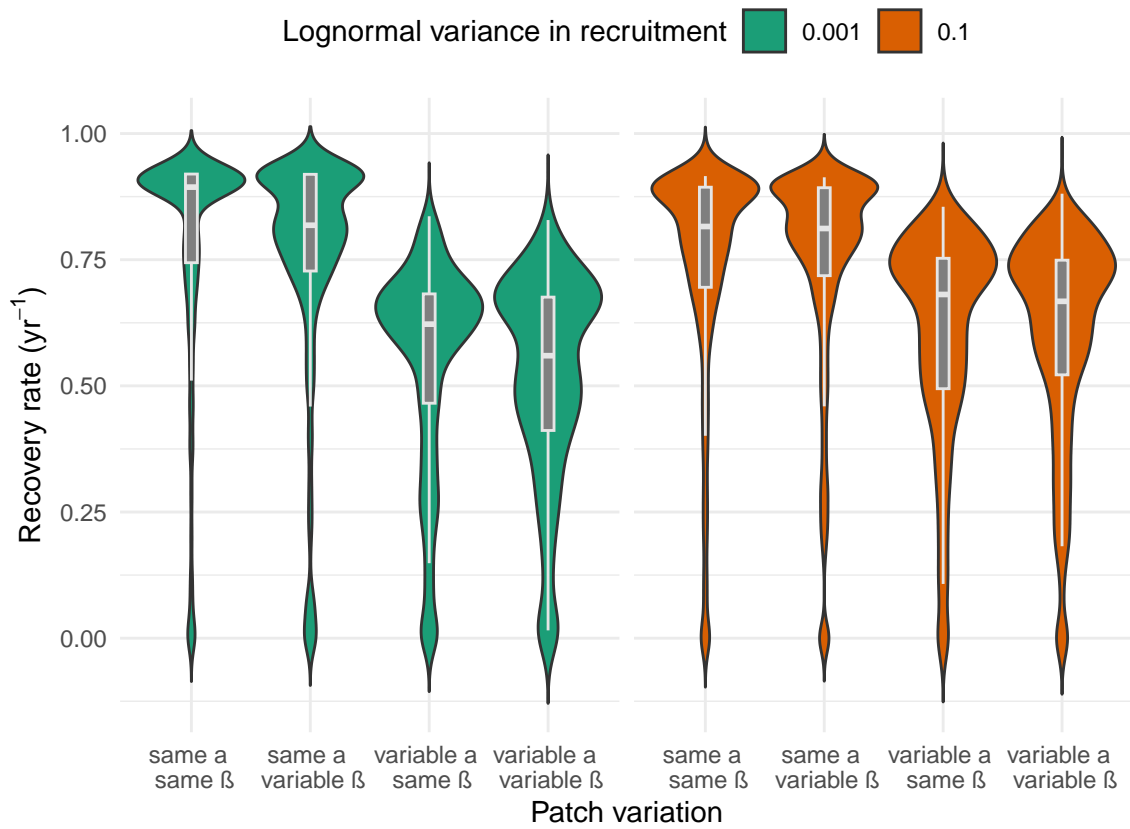
Figure S16: Violin plots indicating the effects of variation among local patch demographic rates on metapopulation recovery across all scenarios. For patch variation, α refers local patch productivity and β denotes local patch carrying capacity.

1.5.3 Clustering analyses

We used hierarchical clustering analyses (implementing Ward's criterion) of a dissimilarity matrix from our four recovery metrics to evaluate whether there was evidence for common recovery regimes among our simulation results across all ecological and disturbance scenarios (Murtagh & Legendre 2014). Based on advice laid out in Hennig (2014), we determined that the best number of unique clusters in metapopulation recoveries should satisfy the following statistical criteria:

1. recovery outcomes from within a cluster are closer to one another than to other clusters (i.e., the two Dunn indices are relatively high)
2. the number of clusters explains much of the point variation within the dataset (i.e., diminishing returns in minimizing the sums-of-squared residuals)
3. the point observations within clusters are relatively tight (i.e., both the average silhouette width and the widest within-cluster gap are relatively low)
4. clusters are relatively unique and there is good separation between the clusters (i.e., the separation index is still high, while considering that low numbers of clusters should always have the highest separation)
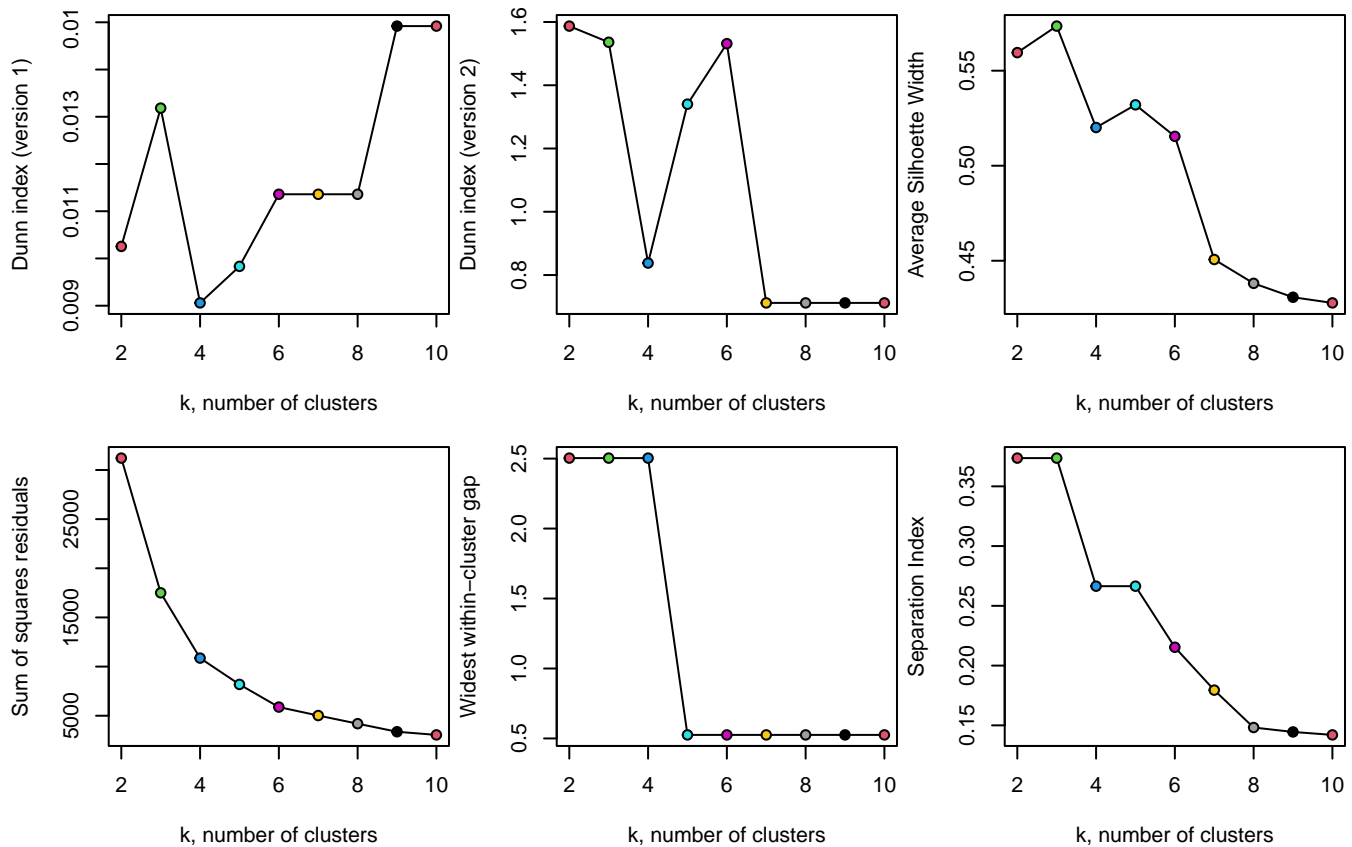
Figure S17: The relationships between number of potential clusters and multiple statistical criteria used to test support for the best number of clusters within the simulated recovery outcomes

Based on the above criteria, we chose 5 unique clusters as satisfying most of the above criteria in the figure above, although there was good support for between 3 and 6 unique clusters. The principal components analysis indicates that five clusters has substantial explanatory power of metapopulation recovery metrics (explained ~89% of the point variation).

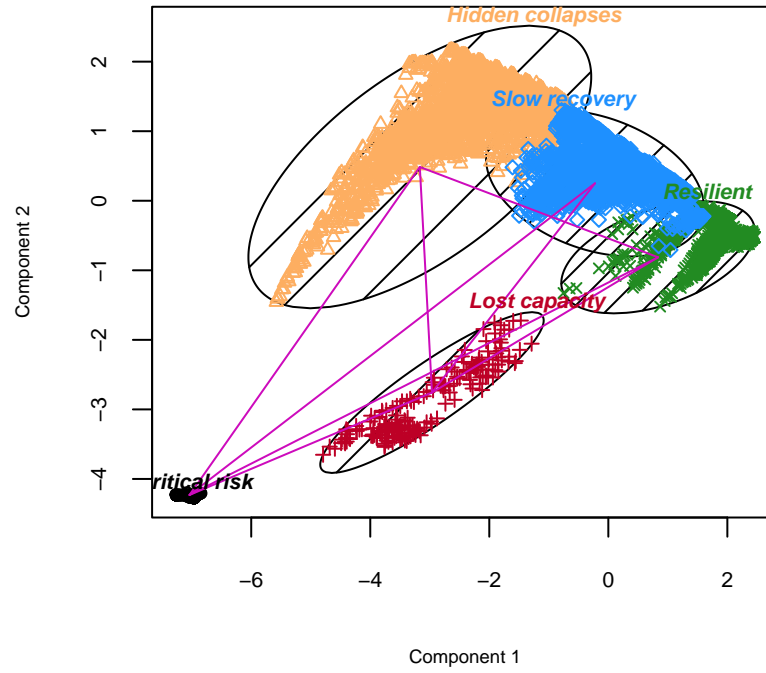Figure S18: Bivariate cluster plot of the principal components explaining point variation in metapopulaton recovery metrics acrosss all simulated scenarios grouped into five distinct clusters.

1.5.4 Emergent recovery outcomes

Overall, we used hierarchical clustering analyses to describe five common metapopulation recovery outcomes. These outcomes were: (1) resilient recovery – metapopulations recovered to pre-disturbance abundances quickly with all patches occupied, (2) slow recovery – metapopulation recovery was slow but there were no other changes in metrics, (3) hidden collapses – metapopulations tended to recover and aggregate abundances were high, but many local patches remained unoccupied and recovery was slowed, (4) lost capacity – recovery rates were very slow, the risk of non-recovery was high, long-term production was low, and many local patches remained unoccupied and (5) critical risk – where metapopulations failed to recover, abundances remained low, and the risk of non-recovery was high.

Table S2: The mean recovery metrics, total sample size per regime (No.), and metapopulation abundance (N/K) for each of five common metapopulation recovery regimes supported by hierarchical clustering analyses across gradients in disturbance and network structure.

Regime	Network	Disturbance	No.	Recovery rate	% non-recovery	Occupancy	Relative production	Relative abundance
Resilient	Linear	Uniform	792	0.83	2	0.99	0.98	1.00
Resilient	Dendritic	Uniform	792	0.82	2	0.99	0.98	0.99
Resilient	Star	Uniform	792	0.81	3	0.99	0.98	0.99
Resilient	Grid	Uniform	792	0.82	2	0.99	0.98	1.00
Resilient	Linear	Local, even	205	0.78	5	0.94	0.95	0.99
Resilient	Dendritic	Local, even	201	0.78	5	0.94	0.96	0.99
Resilient	Star	Local, even	274	0.75	7	0.93	0.95	0.99
Resilient	Grid	Local, even	215	0.78	5	0.94	0.96	0.99
Slow recovery	Linear	Local, even	528	0.69	3	0.77	0.87	0.99
Slow recovery	Dendritic	Local, even	533	0.70	3	0.77	0.87	0.99
Slow recovery	Star	Local, even	466	0.68	5	0.75	0.86	0.99
Slow recovery	Grid	Local, even	529	0.73	3	0.81	0.89	0.99
Slow recovery	Linear	Local, uneven	11	0.72	0	0.64	0.81	1.00
Slow recovery	Dendritic	Local, uneven	69	0.73	0	0.66	0.81	0.99
Slow recovery	Star	Local, uneven	114	0.74	4	0.71	0.84	0.97
Slow recovery	Grid	Local, uneven	244	0.76	0	0.73	0.85	1.00
Hidden collapses	Linear	Local, even	9	0.61	3	0.59	0.79	0.99

Hidden collapses	Dendritic	Local, even	9	0.65	0	0.59	0.78	0.99
Hidden collapses	Star	Local, even	4	0.72	0	0.55	0.76	1.00
Hidden collapses	Linear	Local, uneven	709	0.34	21	0.34	0.67	0.97
Hidden collapses	Dendritic	Local, uneven	651	0.49	8	0.36	0.68	0.99
Hidden collapses	Star	Local, uneven	606	0.57	9	0.45	0.72	0.99
Hidden collapses	Grid	Local, uneven	476	0.56	7	0.46	0.73	0.99
Lost capacity	Linear	Local, even	50	0.17	77	0.58	0.79	0.66
Lost capacity	Dendritic	Local, even	49	0.16	78	0.58	0.78	0.65
Lost capacity	Star	Local, even	48	0.16	78	0.58	0.78	0.65
Lost capacity	Grid	Local, even	48	0.16	79	0.57	0.78	0.64
Critical risk	Linear	Local, uneven	72	0.00	100	0.10	0.54	0.09
Critical risk	Dendritic	Local, uneven	72	0.00	100	0.10	0.54	0.08
Critical risk	Star	Local, uneven	72	0.00	100	0.10	0.54	0.08
Critical risk	Grid	Local, uneven	72	0.00	100	0.10	0.54	0.08

248 These five spatial recovery regimes emerged from the interplay of density-dependent productivity, network
249 structure (shown here), dispersal, stochasticity, and spatial disturbance regimes (Figures S11-S14). Resilient
250 recovery regimes were most common when disturbance was evenly applied across the network and local patches
251 were identical. Any localized disturbances could create poor recovery outcomes, and the frequency of these recovery
252 regimes were often exacerbated when patch demographic rates, like productivity and carrying capacity, varied from
253 one another. Localized, even disturbances tended to reduce recovery rates. The riskiest recovery outcomes emerged
254 when disturbance was localized and allowed for extirpation (Table S2). Last, note that linear networks tended to
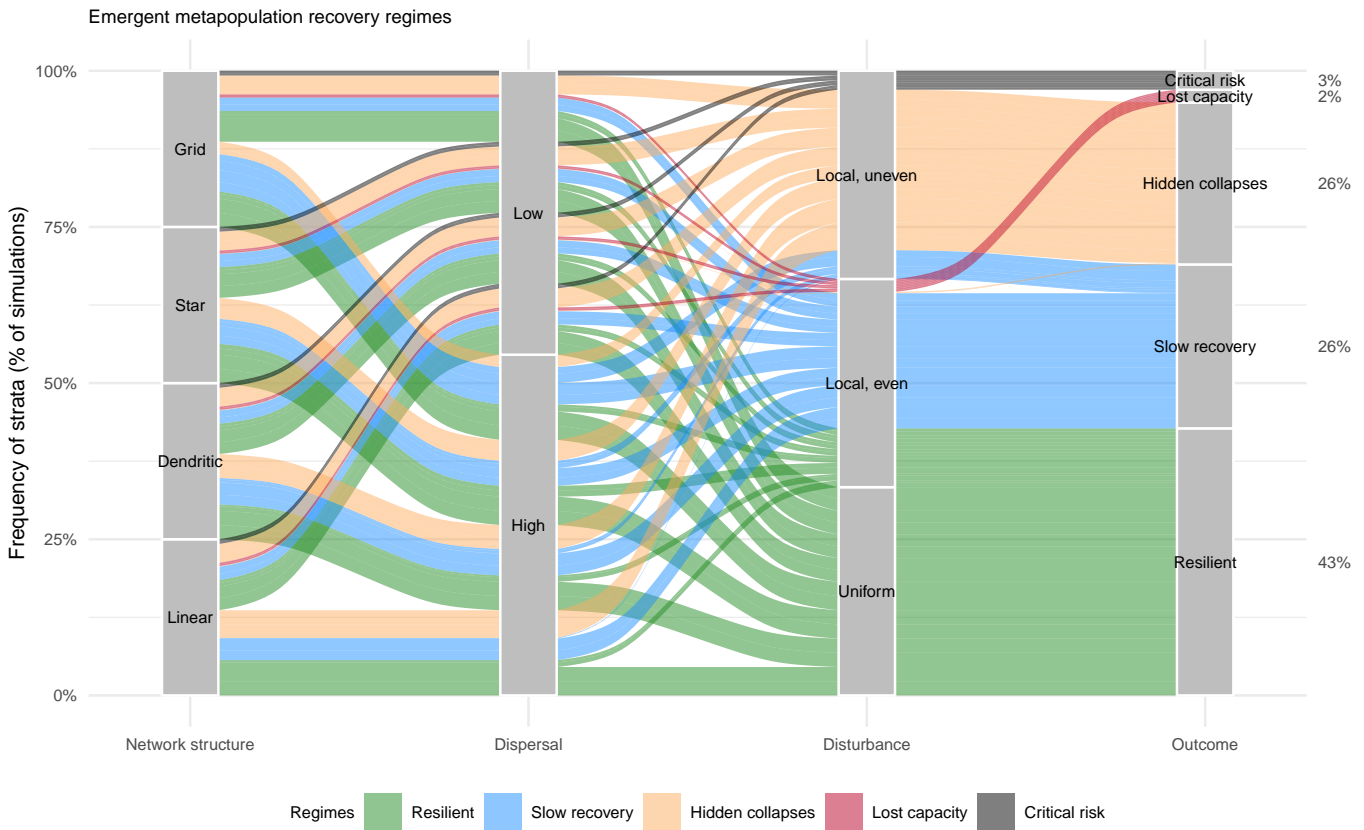255 have higher risks for long-term spatial contractions.

Figure S19: Frequency of emergent metapopulation recovery regimes can depend on a complex interplay between
network structure, dispersal, and spatial disturbances. Ribbon colors denote a group of simulations that led to one
of five common recovery outcomes. Frequency of regimes denoted by width of ribbons

1.6 References

257 Anderson, S.C., Moore, J.W., McClure, M.M., Dulvy, N.K. & Cooper, A.B. (2015). Portfolio conservation of
258   metapopulations under climate change. *Ecological Applications*, 25, 559–572.

Bowlby, H.D. & Gibson, A.J.F. (2020). Evaluating whether metapopulation structure benefits endangered diadromous fishes. *Canadian Journal of Fisheries and Aquatic Sciences*, 77, 388–400.

Csardi, G. & Nepusz, T. (2006). The igraph software package for complex network research. *InterJournal*, Complex Sy, 1695.

Forrest, R.E., McAllister, M.K., Dorn, M.W., Martell, S.J.D. & Stanley, R.D. (2010). Hierarchical Bayesian estimation of recruitment parameters and reference points for Pacific rockfishes (Sebastes spp.) under alternative assumptions about the stock–recruit function. *Canadian Journal of Fisheries and Aquatic Sciences*, 67, 1611–1634.

Fullerton, A.H., Anzalone, S., Moran, P., Van Doornik, D.M., Copeland, T. & Zabel, R.W. (2016). Setting spatial conservation priorities despite incomplete data for characterizing metapopulations. *Ecological Applications*, 26, 2558–2578.

Hennig, C. (2014). How many bee species? A case study in determining the number of clusters. In: *Data analysis, machine learning and knowledge discovery* (eds. Spiliopoulou, M., Schmidt-Thieme, L. & Janning, R.). pp. 41–49.

Moore, J.W., Connors, B.M. & Hodgson, E.E. (2021). Conservation risks and portfolio effects in mixed-stock fisheries. *Fish and Fisheries*, faf.12567.

Murtagh, F. & Legendre, P. (2014). Ward's hierarchical agglomerative clustering method: which algorithms implement Ward's criterion? *Journal of Classification*, 31, 274–295.

Myers, R.A., Bowen, K.G. & Barrowman, N.J. (1999). Maximum reproductive rate of fish at low population sizes. *Canadian Journal of Fisheries and Aquatic Sciences*, 56, 2404–2419.

Okamoto, D.K., Hessing-Lewis, M., Samhouri, J.F., Shelton, A.O., Stier, A.C., Levin, P.S. & Salomon, A.K. (2020). Spatial variation in exploited metapopulations obscures risk of collapse. *Ecological Applications*, 30, e02051.

Walters, C.J. & Martell, S.J.D. (2004). *Fisheries ecology and management.* Princeton University Press.

Yeakel, J.D., Moore, J.W., Guimarães, P.R. & Aguiar, M.A.M. de. (2014). Synchronisation and stability in river metapopulation networks. *Ecology Letters*, 17, 273–283.

Zelnik, Y.R., Arnoldi, J. & Loreau, M. (2019). The three regimes of spatial recovery. *Ecology*, 100, e02586.